

Non-Newtonian Effect on Hemodynamic Characteristics of Blood Flow in Stented Cerebral Aneurysm

Changsheng Huang, Zhenhua Chai and Baochang Shi*

School of Mathematics and Statistics, Huazhong University of Science and Technology, Wuhan 430074, P.R. China.

Received 28 October 2011; Accepted (in revised version) 2 February 2012

Available online 29 August 2012

Abstract. Stent placement is considered as a promising and minimally invasive technique to prevent rupture of aneurysm and favor coagulation mechanism inside the aneurysm. Many scholars study the effect of the stent on blood flow in cerebral aneurysm by numerical simulations, and usually regard blood as the Newtonian fluid, blood, however, is a kind of non-Newtonian fluid in practice. The main purpose of the present paper is to investigate the effect of non-Newtonian behavior on the hemodynamic characteristics of blood flow in stented cerebral aneurysm with lattice Boltzmann method. The Casson model is used to describe the blood non-Newtonian character, which is one of the most popular models in depicting blood fluid. In particular, hemodynamic characteristics derived with Newtonian and non-Newtonian models are studied, and compared in detail. The results show that the non-Newtonian effect gives a great influence on hemodynamic characteristics of blood flow in stented cerebral aneurysm, especially in small necked ones.

AMS subject classifications: 76A05, 76M28, 76D05, 92C35, 74F10

Key words: Cerebral aneurysm, lattice Boltzmann, non-Newtonian fluid, Casson model.

1 Introduction

Cerebral aneurysms are localized dilation or ballooning of the brain blood vessel caused by disease or weakening of the walls. They are particularly dangerous for the risk of permanent brain damage, disability or death when they rupture. A new therapy to treat aneurysm is implanting a porous stent across the neck of the aneurysm, which is viewed as a promising and minimally invasive treatment modality. Many hemodynamic factors,

*Corresponding author. *Email addresses:* hcs013@163.com (C. Huang), hustczh@mail.hust.edu.cn (Z. Chai), shibc@mail.hust.edu.cn (B. Shi)

such as flow patterns, velocity and wall shear stress, are thought to play an important role in the pathogenesis and treatment of cerebral aneurysms [1].

Some studies have investigated the effect of the stent on hemodynamics by experimental methods [2–4]. Lieber et al. [2] investigated the influence of the stent filament size on the intra-aneurysmal flow dynamics in a sidewall aneurysm model *in vitro* using particle image velocimetry. Their results showed that stenting significantly reduces intra-aneurysmal vorticity and the reduction of mean flow circulation varies depending on the strut diameter. Liou et al. [3] investigated the effect of stent shapes (helix versus mesh) on the changes of intra-aneurysmal hemodynamics. They found both stents can induce favorable changes in the intra-aneurysmal flow stasis as well as direction and undulation of wall shear stresses, but the helix stent was more competitive.

Compared to experimental studies, more numerical works examining stent effects on hemodynamics also have been carried out in the past years [5–7]. Aenis et al. [5] conducted a finite element simulation of stented and nonstented aneurysm models in a three-dimensional configuration. The results of the stented versus the nonstented model showed a significant diminution of flow activity inside the stented aneurysm pouch. A high-pressure zone at the distal neck and the dome of the aneurysm prior to stenting decreases after stent placement. Hirabayashi et al. [6] investigated the effect of the stent structure and its positioning on hemodynamics using lattice Boltzmann method (LBM), and found the effects of strut diameter, positioning and aneurism geometry must be taken into account to fully quantify the role of the stent. Appanaboyina et al. [7] studied the effect of stent design, treatment options, stent positioning and partial stent modeling, demonstrated that their methodology based on unstructured embedded grids was useful in simulation of intracranial aneurysm stenting.

The aforementioned studies have provided valuable information on the flow in stented aneurysms, however, most of them assume blood flow to be a Newtonian fluid. It is well accepted that blood behaves as a Newtonian fluid in large arteries where the shear rates above 100 s^{-1} [8]. Nevertheless, the non-Newtonian effect may become important in aneurysms, especially in stented aneurysms with stagnant flow and low shear rates. Some studies have investigated the non-Newtonian effect on hemodynamics in nonstented cerebral aneurysm [9–11]. Bernsdorf et al. [9] simulated blood flow in cerebral aneurysms with lattice Boltzmann method, and showed that there was an overestimation of the wall shear stress results when the non-Newtonian effects were neglected. According to hemodynamic analysis of cerebral aneurysm models with realistic anatomies using Newtonian and non-Newtonian approximations, Cebra et al. [10] showed that the main flow characteristics are not significantly affected by the viscosity model. The results of Fisher and Rossmann's work [11] on the effect of non-Newtonian behavior suggested the blood's non-Newtonian behavior was considerable, but they were not as significant as various aneurysm morphologies, thus the assumption of Newtonian blood is quite reasonable. Furthermore, for stented aneurysm, Kim et al. [12] studied the effect of stent porosity and stent strut shape with a non-Newtonian fluid model for blood, but without a systematic comparison between Newtonian and non-Newtonian blood model.

From discussions previously, it is found that more researches are still required to study the effect of non-Newtonian blood properties on the hemodynamics of flow in stented cerebral aneurism. The objective of this paper is to present a detailed study on the non-Newtonian effect on hemodynamic characteristics of blood flow in stented cerebral aneurism. For simplicity, we only consider two-dimensional cerebral aneurism geometries. The vessel walls are assumed to be rigid, which is partially because some available works have shown that there is no apparent difference on the basic vortex pattern between rigid and distensible saccular aneurisms [13]. The no-slip boundary conditions are used on the vessel walls and the stent surfaces. In addition, we adopt a steady velocity condition as an inlet boundary condition, and consider blood flow to be incompressible.

2 Mathematical model and numerical method for non-Newtonian fluid

2.1 Mathematical model for non-Newtonian fluid

The mathematical model for non-Newtonian fluid flows can be written as

$$\nabla \cdot \mathbf{u} = 0, \quad (2.1a)$$

$$\frac{\partial \mathbf{u}}{\partial t} + \mathbf{u} \cdot \nabla \mathbf{u} = -\nabla P + \nabla \cdot \boldsymbol{\tau}, \quad (2.1b)$$

where \mathbf{u} is fluid velocity, P is the pressure; $\boldsymbol{\tau} = \mu(|\dot{\gamma}|)\dot{\gamma}$ is shear stress, μ is local dynamic viscosity and related to the kinematic viscosity, $\dot{\gamma}$ is shear rate and defined as

$$\dot{\gamma} = 2\varepsilon = \nabla \mathbf{u} + (\nabla \mathbf{u})^T, \quad |\dot{\gamma}| = \sqrt{2(\varepsilon:\varepsilon)}, \quad (2.2)$$

where ε is strain rate tensor, T denotes the transposition operator. Compared with the Navier-Stokes equations for the Newtonian fluid flows, the dynamics viscosity μ in Eq. (2.1) is a function of shear rate $\dot{\gamma}$ rather than a constant.

Although there are many types or models of non-Newtonian fluid [14], here we will use Casson model since this model shows both yield stress and shear-thinning non-Newtonian viscosity, and also broadly used to describe the shear thinning behavior of blood [15, 16]. The shear stress of Casson model can be described as [14, 17]

$$\begin{cases} \boldsymbol{\tau} = \left(\sqrt{\frac{\tau_C}{|\dot{\gamma}|}} + \sqrt{\mu_C} \right)^2 \dot{\gamma}, & |\boldsymbol{\tau}| > \tau_C, \\ \dot{\gamma} = 0, & |\boldsymbol{\tau}| < \tau_C, \end{cases} \quad (2.3)$$

where τ_C is the Casson yield stress, μ_C is the plastic viscosity, the magnitude of the shear stress is defined as

$$|\boldsymbol{\tau}| = \sqrt{\frac{1}{2}(\boldsymbol{\tau}:\boldsymbol{\tau})}. \quad (2.4)$$

Following the approach proposed by Papanastasiou [18], one can derive a continuous expression on shear stress [17, 19]

$$\tau = \left[\sqrt{\mu_C} + (1 - e^{-\sqrt{m|\dot{\gamma}|}}) \sqrt{\frac{\tau_C}{|\dot{\gamma}|}} \right]^2 \dot{\gamma}, \quad (2.5)$$

which can be used to eliminate the difficulties induced by discontinuity of Eq. (2.3). Parameter m is a constant, for $m > 100$, Eq. (2.5) gives a good approximation to Eq. (2.3), as reported in [19]. Additionally Eq. (2.5) also can be used to describes a Newtonian fluid if $\tau_C = 0$.

Based on Eq. (2.5), the apparent or effective viscosity for Casson model can be written as follow,

$$\mu_{CS} = \left[\sqrt{\mu_C} + (1 - e^{-\sqrt{m|\dot{\gamma}|}}) \sqrt{\frac{\tau_C}{|\dot{\gamma}|}} \right]^2. \quad (2.6)$$

2.2 The lattice Boltzmann method for non-Newtonian fluid

The lattice Boltzmann method has been proved to be a very efficient simulation tool to model complex fluids [20, 21], and has been widely used in simulation of blood flow [22, 23]. A popular lattice Boltzmann model is the so-called Bhatnagar-Gross-Krook (BGK) model with a single relaxation time approximation. The evolution equation of BGK model can be given as [24]

$$f_i(\mathbf{x} + \mathbf{c}_i \delta t, t + \delta t) - f_i(\mathbf{x}, t) = -\frac{1}{\tau_{BGK}} \left[f_i(\mathbf{x}, t) - f_i^{(eq)}(\mathbf{x}, t) \right], \quad (2.7)$$

where τ_{BGK} is the dimensionless relaxation time, $f_i(\mathbf{x}, t)$ is the density distribution function for the particle moving with velocity \mathbf{c}_i at position \mathbf{x} and time t , $f_i^{(eq)}(\mathbf{x}, t)$ is the local equilibrium distribution function. For the two-dimensional case considered in the present work, a two-dimensional lattice Boltzmann model with nine velocities (D2Q9 model) will be used. The local equilibrium distribution function in the D2Q9 model is defined as [24]

$$f_i^{(eq)}(\mathbf{x}, t) = \omega_i \rho \left[1 + \frac{\mathbf{c}_i \cdot \mathbf{u}}{c_s^2} + \frac{(\mathbf{c}_i \cdot \mathbf{u})^2}{2c_s^4} - \frac{|\mathbf{u}|^2}{2c_s^2} \right], \quad (2.8)$$

where ω_i is the weighting factor given by $\omega_0 = 4/9$, $\omega_i = 1/9 (i = 1:4)$, $\omega_i = 1/36 (i = 5:8)$, ρ , \mathbf{u} are the fluid density and velocity, c_s is the sound speed. The discrete velocities \mathbf{c}_i are defined as

$$\mathbf{c}_i = \begin{cases} (0,0), & i=0, \\ (\cos[(i-1)\pi/2], \sin[(i-1)\pi/2])c, & i=1-4, \\ (\cos[(2i-9)\pi/4], \sin[(2i-9)\pi/4])\sqrt{2}c, & i=5-8, \end{cases} \quad (2.9)$$

where $c = \delta x / \delta t$, and δx and δt are the lattice spacing and time step. The relation between c_s and c can be expressed as $c_s = c / \sqrt{3}$. The flow density, velocity and kinetic viscosity are given by

$$\rho(\mathbf{x}, t) = \sum_{i=0}^8 f_i(\mathbf{x}, t), \quad (2.10a)$$

$$\rho(\mathbf{x}, t) \mathbf{u}(\mathbf{x}, t) = \sum_{i=0}^8 \mathbf{c}_i f_i(\mathbf{x}, t), \quad (2.10b)$$

$$\nu = (\tau_{BGK} - 1/2) c_s^2 \delta t. \quad (2.10c)$$

As reported in some published works [14, 25, 26], the strain rate tensor ε in D2Q9 model can be computed locally at each node by

$$\varepsilon_{\alpha\beta} = -\frac{1}{2\rho c_s^2 \tau_{BGK} \delta t} \sum_{i=0}^8 \mathbf{c}_{i\alpha} \mathbf{c}_{i\beta} [f_i(\mathbf{x}, t) - f_i^{eq}(\mathbf{x}, t)], \quad (2.11)$$

and the shear stress can be further derived

$$\tau_{\alpha\beta} = -\left(1 - \frac{1}{2\tau_{BGK}}\right) \sum_{i=0}^8 \mathbf{c}_{i\alpha} \mathbf{c}_{i\beta} [f_i(\mathbf{x}, t) - f_i^{eq}(\mathbf{x}, t)], \quad (2.12)$$

3 Results and discussions

In this work, we only consider two types of aneurysm geometry with different neck size, and show them in Fig. 1. We note that the two ideal models have been widely used in some previous works [6, 27] for its simplicity and good approximation to realistic cases observed in clinical experiments. The aneurysm diameter is 10mm, the orifice diameters of the large-necked aneurysm (La model) and the small-necked aneurysm (Sa model) are 10mm and 5mm, respectively. The parent vessel is assumed to be a straight tube, the diameter is 4mm and the length is 40mm. Two kinds of stent with different porosities (metal free area/total unit area) represented in Table 1 are used in our simulations. The length and diameter of them are 25mm and 0.1mm. We note that these parameters of stents are also adopted in the work of Hirabayashi et al. [6] and Kim et al. [12].

Table 1: Stent parameters for the simulation (in lattice units).

Stent model	Pore size	Porosity(%)
Ls	35	95.51
Ss	15	89.53

The density of the blood, Casson viscosity and yield stress are $1.087 \times 10^3 \text{ kg/m}^3$, $3.695 \times 10^{-3} \text{ pa}\cdot\text{s}$ and 0.05 dyn/cm^2 , respectively. To simplify numerical study, the following non-dimensionalized parameters are used in the present work. The average density

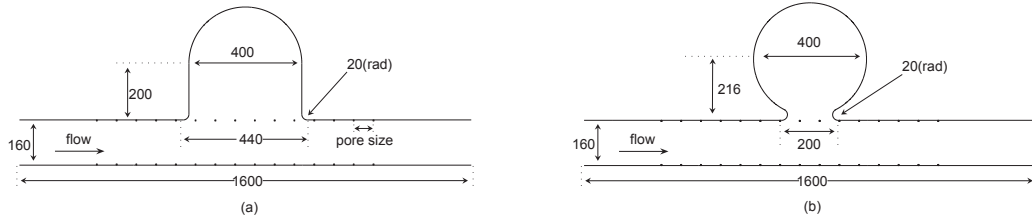


Figure 1: The geometry of aneurysms; (a) the large-necked (La) model, (b) the small-necked (Sa) model.

is $\rho = 1.0$, Casson viscosity $\nu = 0.026$, and yield stress is 6.73×10^{-7} . The non-equilibrium extrapolation method [28] is applied to treat pressure conditions at the inlet and outlet with constant pressure gradient $dP/dx = 4.17 \times 10^{-6}$. For the stent surfaces as well as the vessel walls, the half-way bounce-back condition [29] is used.

3.1 Validation

Firstly, to validate the capacity of present numerical method in studying non-Newtonian behavior, the problem of fully developed channel flow driven by a constant pressure gradient is used here. The reason for choosing such problem is that it has an analytical solution. The exact solution of channel flow with the Casson model is [30]

$$u(y) = \frac{1}{\mu_c} \frac{dP}{dx} \left(\frac{y(y-L)}{2} + y_c \left(\left| y - \frac{L}{2} \right| - \frac{L}{2} \right) - \frac{4}{3} \sqrt{y_c} \left(\sqrt{\left(y - \frac{L}{2} \right)^3 - \sqrt{L^3}} \right) \right), \quad (3.1)$$

where $y_c = -\tau_c / (\frac{\partial P}{\partial x})$ denotes the point at which the material yields. In the simulations, the lattice size used is $N_x \times N_y = 33 \times 17$. The simulation parameters is the same that represent in previous paragraph. Fig. 2 shows that the numerical results agree well with the analytical solutions for both Newtonian and Casson models. The second validation is presented in Fig. 3(b) where we simulated the aneurysm model demonstrated in Fig. 3(a) where the porosity of stent is 95.51%, and compared with the numerical results given by Kim et al. [12]. The results presented in Fig. 3(b) show that the present results are in good agreement with the work of Kim et al. [12]. The grid-independence study shows that 1600×576 lattice size is enough to give accurate results, and this lattice size is used in following simulations.

3.2 Non-Newtonian effect on flow patterns and vortex

The variation of the flow patterns in stented and nonstented aneurysms under the assumption of Newtonian fluid is shown in Fig. 4. Fig. 4(a)-(c) show the streamline in aneurysm La model, and Fig. 4(d)-(f) show that in Sa model. Fig. 4(a) and Fig. 4(d) are cases without stent, while Fig. 4(b), Fig. 4(e) and Fig. 4(c), Fig. 4(f) are cases with high-

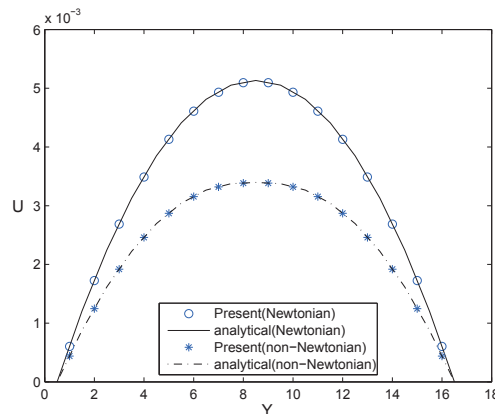


Figure 2: A comparison between numerical and exact velocity profiles for Newtonian and Casson models.

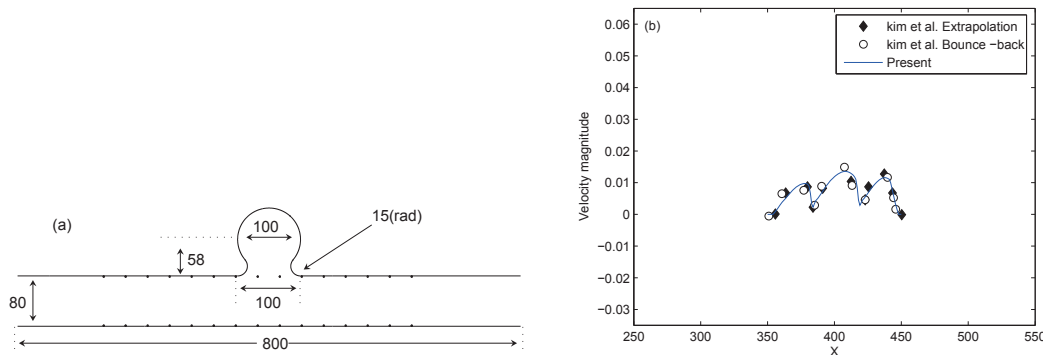


Figure 3: (a)The geometry of the aneurysm model used by Kim et al.; (b) A comparison of the velocity magnitude at the neck of the aneurysm with Kim's results.

and low-porosity stents. As seen from Fig. 4, the flow pattern in the aneurysm with stent is more complex compared to the case without stent, and it seems that the change of flow pattern is more significant for large-necked aneurysm. We also find that the strength of vortex appeared in the aneurysm with stent is much smaller than the cases without stent. In addition, we also note that our results do not agree with the work of Hirabayashi et al. [6] well, this may be because the lattice size they used in their simulations is not large enough, and thus, a large error is induced when the standard bounce-back condition is used on the stent surfaces.

In what follows, we also study the non-Newtonian effect on flow patterns. The numerical results using Casson model for the same cases in Fig. 4 are shown in Fig. 5. As presented in this figure, we find the strength of the vortex is also reduced after the placement of stent, which is similar to the results in Fig. 4. However, many differences are also observed in comparison with the results derived with Newtonian model. Although the

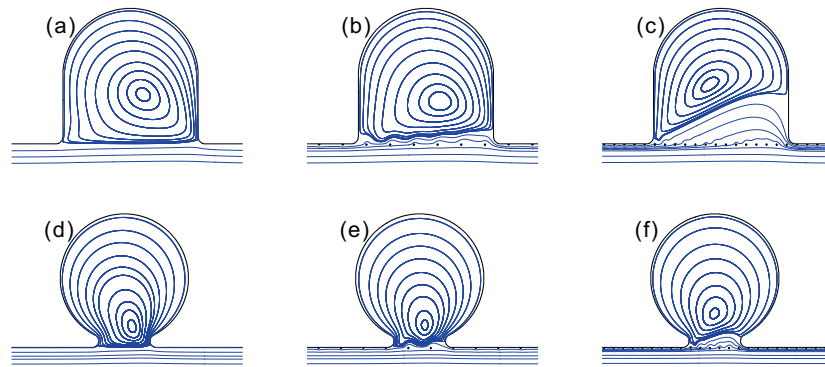


Figure 4: Streamline of the flow inside different aneurysms (Newtonian model). (a) and (d) are non-stented cases, (b), (e) and (c), (f) are cases with high- and low-porosity stents. The aneurysm presented in Fig. 4(a)-(c) is La model, while in Fig. 4(d)-(f) is Sa model.

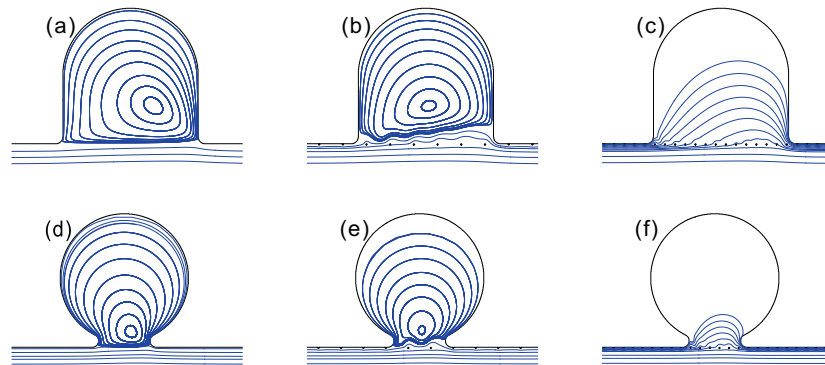


Figure 5: Streamline of the flow inside different aneurysms (non-Newtonian model). (a) and (d) are non-stented cases, (b), (e) and (c), (f) are cases with high- and low-porosity stents. The aneurysm presented in Fig. 5(a)-(c) is La model, while in Fig. 5(d)-(f) is Sa model.

flow patterns in Fig. 5(a), (b) and (d) are very similar to those in Fig. 4, the rest results in Fig. 5(c), (e) and (f) are very different with corresponding cases in Fig. 4. At the dome of the aneurysm in Fig. 5(c), Fig. 5(e) and Fig. 5(f), there is no streamline since the velocity is zero. This means the stagnancy of blood, which is beneficial to the formation of thrombosis in the aneurysm. While in Fig. 4, this phenomenon doesn't appear. The most significant differences is found between the cases with low-porosity stent. In Fig. 5(c) and (f), the vortex disappeared while for the same cases in Fig. 4(c) and (f), the vortex still existed. The flow entered the aneurysm sac through the proximal neck, while in Fig. 4(c) and (f), the flow into the aneurysm from the distal neck.

The most apparent changes taking place for the cases with low-porosity suggest that, as the porosity of the stent become lower, the effect of non-Newtonian behavior become

more significant, this maybe partially because the velocity of blood is greatly reduced and thus, the shear rates become lower. The little difference between Fig. 4(b) and Fig. 5(b) gives an implication that large-necked aneurysm is less sensitive to the non-Newtonian behavior than small-necked aneurysm, as expected.

3.3 Non-Newtonian effect on velocity and flow reduction

To quantitatively evaluate non-Newtonian effect, the mean and the maximum velocity magnitudes inside the aneurysm are computed with Newtonian and Casson models, and reported in Table 2. Based on the data in this table, we find that the velocity of the flow in the aneurysm is reduced after the stent implantation for both Newtonian and Casson models. However, the mean and the maximum velocity magnitudes of Casson model are smaller than these of Newtonian model. This suggest that there is an overestimation of the velocity magnitude inside the aneurysm when blood is treated as Newtonian fluid. In addition, we also observed that the difference between Newtonian and Casson models is more obvious for small-necked aneurysm than that for large-necked aneurysm, which also indicates that the blood is more likely to behave as a non-Newtonian fluid in small-necked aneurysm.

Table 2: The mean and the maximum velocity magnitude calculated inside the aneurysm, and the mean velocity reduction for both models.

Aneurysm	Large-necked			Small-necked		
	-	Ls	Ss	-	Ls	Ss
Max (Newtonian)	0.0415	0.0228	0.0181	0.0255	0.0150	0.0077
Max (Casson)	0.0395	0.0225	0.0164	0.0238	0.0136	0.0066
Relative difference	5%	1%	9%	6%	9%	14%
Mean (Newtonian)	0.00819	0.00273	0.00091	0.00184	0.00082	0.00023
Mean (Casson)	0.00608	0.00201	0.00085	0.00114	0.00040	0.00010
Relative difference	26%	26%	6%	38%	51%	57%
Reduction (Newtonian)	-	66.7%	88.9%	-	55.4%	87.5%
Reduction (Casson)	-	66.7%	86.0%	-	64.9%	91.2%

To measure the effect of stent, the mean velocity reduction is a widely used indicator, and defined as

$$V_r = \frac{V_{ns} - V_{st}}{V_{ns}} \times 100, \quad (3.2)$$

where V_{st} and V_{ns} are the average velocity in the stented and non-stented aneurysm sac, respectively. The mean velocity reduction is also shown in Table 2. As seen from this table, we also find that the placement of stent indeed reduces the velocity in the aneurysm, it's more distinct for the case of Ss.

3.4 Non-Newtonian effect on wall shear stress

Wall shear stress (WSS) is one of the main pathogenic factors correlated with aneurysm expansion and rupture. In this part, we also study WSS of large-necked aneurysm, and show its distribution in Fig. 6. Four cases are shown in the figure: the case with high-porosity stent or without stent, using Newtonian or Casson model. From this figure, it is found that the value of WSS is very small and close to zero except for the regions near the proximal and distal necks, where two peaks appear. The maximum WSS appears at the distal neck region, this may be caused by the impact of the inflow. Compared with the aneurysm without stent, the magnitude of WSS of the stented case is reduced particularly at the zone close to the distal neck. These phenomena were also observed in the work of Yu et al. [31]. In addition, high WSS is also found on the surface of the stent, which is induced by a large velocity gradient.

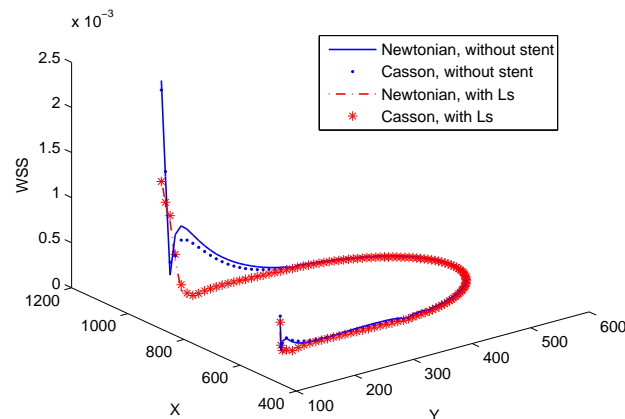


Figure 6: Wall shear stress for large-necked aneurysm in four cases: the case with high-porosity stent or without stent, using Newtonian or Casson model.

Similar to the result of Bernsdorf et al. [9] and Xiang et al. [32], a smaller value of WSS appeared in nonstented case where the Casson model is used. The most significant difference between Newtonian and Casson models is observed at the zone near the distal neck (see Fig. 6), which is due to the fact that abrupt change of velocity as the inflow impacted on the distal neck region and a flatter velocity profile when considering non-Newtonian behavior. While in the stented cases, the difference is much smaller between the two models, this maybe as a result of lower velocity magnitude, which is caused by the stent. The results for small-necked aneurysm exhibit the same phenomenon as those for large-necked aneurysm, and are not shown here.

4 Conclusions

In this paper, we preliminarily studied the hemodynamic characteristics of stented cerebral aneurysm in simplified two-dimensional geometries, and focus on the effect of non-

Newtonian behavior. The results derived with Newtonian and non-Newtonian models were compared, and many differences were found. Firstly, the flow pattern is changed greatly for the cases with low-porosity stent after taking into account the effect of non-Newtonian behavior, while for the non-stented aneurysm, or the aneurysm with high-porosity stent implanted, the difference is very small. Secondly, the mean and the maximum velocity magnitudes in the aneurysm sac were also compared, the values derived with Casson model is much smaller than that obtained with Newtonian model. Thirdly, the value of wall shear stress derived with Casson model is lower than that of Newtonian model, and the maximum difference appeared at the region close to the distal neck. While for the stented cases, a much smaller difference was observed between Newtonian and Casson models.

Our research shows that, it may be not appropriate to treat blood as a Newtonian fluid in the stented aneurysm, this is because the flow pattern and velocity magnitude of the Newtonian and non-Newtonian models present some apparent differences. We also find that the small-necked aneurysm is more sensitive to non-Newtonian behavior since there is a more significant change in flow pattern and velocity magnitude. Our future work will consider three-dimensional, patient-specific aneurysm models and pulsating flow, which will be more realistic.

Acknowledgments

This work is financially supported by the National Natural Science Foundation of China (Grant Nos. 51006040, and 51006039), and the Fundamental Research Funds for the Central Universities, HUST (Grant Nos. 2010QN057 and 2010MS131).

References

- [1] G. N. Foutarakis, H. Yonas and R. J. Scwabassi, Saccular aneurysm formation in curved and bifurcating arteries, *AJNR Am. J. Neuroradiol.*, 20 (1999), 1309-1317.
- [2] B. B. Lieber, V. Livescu, L. N. Hopkins and A. K. Wakhloo, Particle image velocimetry assessment of stent design influence on intra-aneurysmal flow, *Ann. Biomed. Eng.*, 30 (2002), 768-777.
- [3] T. M. Liou, S. N. Liou and K. L. Chu, Intra-aneurysmal flow with helix and mesh stent placement across side-wall aneurysm pore of a straight parent vessel, *J. Biomech. Eng.*, 126 (2004), 36-43.
- [4] K. Barath, F. Cassot, J. H. D. Fasel, M. Ohta and D. A. Rüfenacht, Influence of stent properties on the alteration of cerebral intra-aneurysmal haemodynamics: flow quantification in elastic sidewall aneurysm models, *Neurol. Res.*, 27 (2005), 120-128.
- [5] M. Aenis, A. P. Stancampiano, A. K. Wakhloo and B. B. Lieber, Modeling of flow in a straight stented and nonstented side wall aneurysm model, *J. Biomech. Eng.*, 119 (1997), 206-212.
- [6] M. Hirabayashi, M. Ohta, D. A. Rüfenacht and B. Chopard, A lattice Boltzmann study of blood flow in stented aneurism, *Future Gener. Comp. Sy.*, 20 (2004), 925-934.

- [7] S. Appanaboyina, F. Mut, R. Löhner, C. Putman and J. R. Cebal, Simulation of intracranial aneurysm stenting: techniques and challenges, *Comput. Methods Appl. Mech. Eng.*, 198 (2009), 3567-3582.
- [8] S. A. Berger and L. D. Jou, Flows in stenotic vessels, *Annu. Rev. Fluid Mech.*, 32 (2000), 347-382.
- [9] J. Bernsdorf and D. Wang, Non-Newtonian blood flow simulation in cerebral aneurysms, *Comput. Math. Appl.*, 58 (2009), 1024-1029.
- [10] J. R. Cebal, M. A. Castro, S. Appanaboyina, C. M. Putman, D. Millan and A. F. Frangi, Efficient pipeline for image-based patient-specific analysis of cerebral aneurysm hemodynamics: technique and sensitivity, *IEEE Trans. Med. Imaging*, 24 (2005), 457-467.
- [11] C. Fisher and J. S. Rossmann, Effect of non-Newtonian behavior on hemodynamics of cerebral aneurysms, *J. Biomech. Eng.*, 131 (2009), 91004.
- [12] Y. H. Kim, X. Xu and J. S. Lee, The effect of stent porosity and strut shape on saccular aneurysm and its numerical analysis with lattice Boltzmann method, *Ann. Biomed. Eng.*, 38 (2010), 2274-2292.
- [13] M. Löw, K. Perktold and R. Raunig, Hemodynamics in rigid and distensible saccular aneurysms: a numerical study of pulsatile flow characteristics, *Biorheology*, 30 (1993), 287-298.
- [14] Z. Chai, B. Shi, Z. Guo and F. Rong, Multiple-relaxation-time lattice Boltzmann model for generalized Newtonian fluid flows, *J. Non-Newton. Fluid Mech.*, 166 (2011), 332-342.
- [15] Y. Ji, X. Kang and D. Liu, Simulation of non-Newtonian blood flow by lattice Boltzmann method, *Chinese Phys. Lett.*, 27 (2010), 94701-94704.
- [16] R. Ouared and B. Chopard, Lattice Boltzmann simulations of blood flow: non-Newtonian rheology and clotting processes, *J. Stat. Phys.*, 121 (2005), 209-221.
- [17] P. Neofytou, A 3rd order upwind finite volume method for generalised Newtonian fluid flows, *Adv. Eng. Softw.*, 36 (2005), 664-680.
- [18] T. C. Papanastasiou, Flows of materials with yield, *J. Rheol.*, 31 (1987), 385-404.
- [19] T. V. Pham and E. Mitsoulis, Entry and exit flows of Casson fluids, *Can. J. Chem. Eng.*, 72 (1994), 1080-1084.
- [20] S. Chen and G. D. Doolen, Lattice Boltzmann method for fluid flows, *Annu. Rev. Fluid Mech.*, 30 (1998), 329-364.
- [21] S. Succi, *The lattice Boltzmann equation for fluid dynamics and beyond*, Oxford University Press, USA, 2001.
- [22] S. Melchionna, M. Bernaschi, S. Succi, E. Kaxiras, F.J. Rybicki, D. Mitsouras, A.U. Coskun and C.L. Feldman, Hydrokinetic approach to large-scale cardiovascular blood flow, *Comput. Phys. Comm.*, 181 (2010) 462-472.
- [23] S. Melchionna, A model for red blood cells in simulations of large-scale blood flows, *Macromol. Theory and Sim.*, 20 (2011) 548-561.
- [24] Y. H. Qian, D. D'Humières and P. Lallemand, Lattice BGK model for Navier-Stokes equation, *Europhys. Lett.*, 17 (1992), 479-484.
- [25] J. Boyd, J. Buick and S. Green, A second-order accurate lattice Boltzmann non-Newtonian flow model, *J. Phys. A: Math. Gen.*, 39 (2006), 14241-14247.
- [26] G. H. Tang, X. F. Li, Y. L. He and W. Q. Tao, Electroosmotic flow of non-newtonian fluid in microchannels, *J. Non-Newton. Fluid Mech.*, 157 (2009), 133-137.
- [27] M. Hirabayashi, M. Ohta, D. A. Rüfenacht and B. Chopard, Characterization of flow reduction properties in an aneurysm due to a stent, *Phys. Rev. E*, 68 (2003), 21918.
- [28] Z. Guo, C. Zheng and B. Shi, Non-equilibrium extrapolation method for velocity and pres-

- sure boundary conditions in the lattice Boltzmann method, *Chinese Phys.*, 11 (2002), 366-374.
- [29] X. He, Q. Zou, L.S. Luo and M. Dembo, Analytic solutions of simple flows and analysis of nonslip boundary conditions for the lattice Boltzmann BGK model, *J. Stat. Phys.*, 87 (1997), 115-136.
- [30] M. Ashrafizaadeh and H. Bakhshaei, A comparison of non-Newtonian models for lattice Boltzmann blood flow simulations, *Comput. Math. Appl.*, 58 (2009), 1045-1054.
- [31] S. C. M. Yu and J. B. Zhao, A steady flow analysis on the stented and non-stented sidewall aneurysm models, *Med. Eng. Phys.*, 21 (1999), 133-141.
- [32] J. Xiang, M. Tremmel, J. Kolega, E.I. Levy, S.K. Natarajan and H. Meng, Newtonian viscosity model could overestimate wall shear stress in intracranial aneurysm domes and underestimate rupture risk, *J. NeuroInterv. Surg.* (2011). doi:10.1136/neurintsurg-2011-010089.